

# Space charge neutralization in inertial electrostatic confinement plasmas

E. G. Evstatiev, R. A. Nebel, L. Chacón, J. Park, and G. Lapenta

Citation: *Physics of Plasmas* **14**, 042701 (2007); doi: 10.1063/1.2711173

View online: <https://doi.org/10.1063/1.2711173>

View Table of Contents: <http://aip.scitation.org/toc/php/14/4>

Published by the [American Institute of Physics](#)

---

## Articles you may be interested in

[Periodically oscillating plasma sphere](#)

*Physics of Plasmas* **12**, 056315 (2005); 10.1063/1.1888822

[Inertial-Electrostatic Confinement of Ionized Fusion Gases](#)

*Journal of Applied Physics* **38**, 4522 (1967); 10.1063/1.1709162

[Fusion energy in an inertial electrostatic confinement device using a magnetically shielded grid](#)

*Physics of Plasmas* **22**, 102705 (2015); 10.1063/1.4933213

[On the Inertial-Electrostatic Confinement of a Plasma](#)

*The Physics of Fluids* **2**, 239 (1959); 10.1063/1.1705917

[A general critique of inertial-electrostatic confinement fusion systems](#)

*Physics of Plasmas* **2**, 1853 (1995); 10.1063/1.871273

[Measurement of electron density in a cylindrical inertial electrostatic plasma confinement device](#)

*Journal of Applied Physics* **44**, 5347 (1973); 10.1063/1.1662154

---

PHYSICS TODAY

WHITEPAPERS

ADVANCES IN PRECISION  
MOTION CONTROL

Piezo Flexure Mechanisms  
and Air Bearings

READ NOW

PRESENTED BY

PI

## Space charge neutralization in inertial electrostatic confinement plasmas

E. G. Evstatiev, R. A. Nebel, L. Chacón, J. Park, and G. Lapenta  
*Los Alamos National Laboratory, Los Alamos, New Mexico 87545*

(Received 26 October 2006; accepted 1 February 2007; published online 5 April 2007)

A major issue for electron injected inertial electrostatic confinement (IEC) devices is space charge neutralization. A new formalism is developed that will allow this neutralization to occur for both oscillating and steady-state IEC plasmas. Results indicate that there are limits on the amount of compression that can be achieved by oscillating plasmas while simultaneously maintaining space charge neutralization and parabolic background potential. For steady-state plasmas, there are no such limits and space charge neutralization can be achieved even when the plasma becomes quasineutral. © 2007 American Institute of Physics. [DOI: 10.1063/1.2711173]

### I. INTRODUCTION

Inertial electrostatic confinement (IEC) schemes for fusion devices have been studied both experimentally and theoretically for some 40 years. Purely electrostatic systems<sup>1–4</sup> and combinations of magnetic and electrostatic systems<sup>5–8</sup> have been explored. IEC schemes rely on accelerating ions to a fusion relevant energy range (50–150 KeV) using electric fields. The accelerating fields can be provided by grids<sup>3,4</sup> or virtual cathodes.<sup>1,2,5–10</sup> Either spherical or cylindrical grids with high transparency are used with dc or low-frequency electric fields. Although IECs have demonstrated significant neutron yields (as high as  $2 \times 10^{10}$  neutrons/s in steady state)<sup>4</sup> in a compact (table-top size) and inexpensive device, the fusion reactions are from nonthermal ions. Theoretical studies using simple analytic models have indicated that such systems cannot scale to net energy producing devices.<sup>11,12</sup> However, these studies have several approximations, and a more complete study using a bounce averaged Fokker-Planck model indicated that if the ion distributions are close enough to thermal, net energy gains are possible, although the fusion power densities are small.<sup>13</sup> The underlying problem is that for nonthermal systems, the Coulomb scattering cross sections are larger than the fusion cross sections. Thus, it can take more energy to maintain the nonthermal distributions than the device produces in fusion power.

This problem is avoided if the ion component of the plasma is in local thermodynamic equilibrium (LTE). Both oscillating<sup>14,15</sup> and steady-state plasmas<sup>15</sup> can be in LTE. Oscillating plasmas were suggested as a possible fusion scheme in the theoretical works by Barnes and Nebel.<sup>14,15</sup> A tiny oscillating ion cloud (referred to as the periodically oscillating plasma sphere, or POPS) may undergo a self-similar collapse in a harmonic-oscillator potential formed by uniform electron background. By tuning the external radiofrequency (rf) electric fields to this naturally occurring mode, it is then possible to heat the ions to obtain very high densities and temperatures simultaneously during the collapse phase of the oscillation through adiabatic compression. Theoretical projections indicate that such a scheme is highly effective and may result in net fusion energy gain even for an advanced fuel such as D-D.<sup>15</sup> Recent experimental studies have con-

firmed the existence of the oscillating plasma.<sup>16,17</sup> The experimental setup that observed the oscillations is shown in Fig. 1. The proper scaling of the oscillations with both the ion mass and the potential well depth has been observed.

A major issue that remains is how much plasma compression can be achieved by the POPS oscillations. In order to achieve significant fusion gain in D-D, the required compressions are large ( $\sim 1000:1$  in radius).<sup>15</sup> The original work assumed that there would be enough cold electrons in the plasma to space charge neutralize the plasma sphere as it compressed.<sup>14,15</sup> More recent work has verified that this effect does occur<sup>17</sup> but it is not strong enough to completely space charge neutralize the sphere as it collapses. However, by properly programming the distribution function of the injected electrons, it is possible to significantly improve the space charge neutralization and the plasma compression.<sup>17</sup> (It should be noted that previous work has demonstrated that the shape of the injected electron distribution function can be controlled on the experiment.<sup>18,19</sup>)

Steady-state IEC plasmas are based on ion heating in a uniform electron background. Fusion densities are reached by operating in the quasineutral limit ( $n_i \sim n_e$ ) rather than through large compressions.<sup>15</sup> These systems also need precise control of the electron distribution in order to simultaneously maintain quasineutrality and provide a confining potential for the ions. Although compression is not an issue for these plasmas, stability can be.<sup>1</sup> Steady-state plasmas of this kind have not been studied in depth. The formalism developed in this paper applies to these plasmas as well as to the oscillating ones.

In the present work, a systematic approach is taken in order to determine how to best inject electrons into an IEC system of the above two kinds. A new formalism (based on the formalism presented in Ref. 20) is developed that prescribes how to program the injected electron velocity distribution on the boundary in order to achieve any prescribed static (slowly time-varying or time-independent) density profile in a harmonic-oscillator potential. This formalism is presented in Sec. II. Section III applies the new formalism to POPS compressions. The formalism is incorporated into the one-dimensional gridless particle code ENNF<sup>21</sup> and a plasma compression is simulated. Although the formalism works

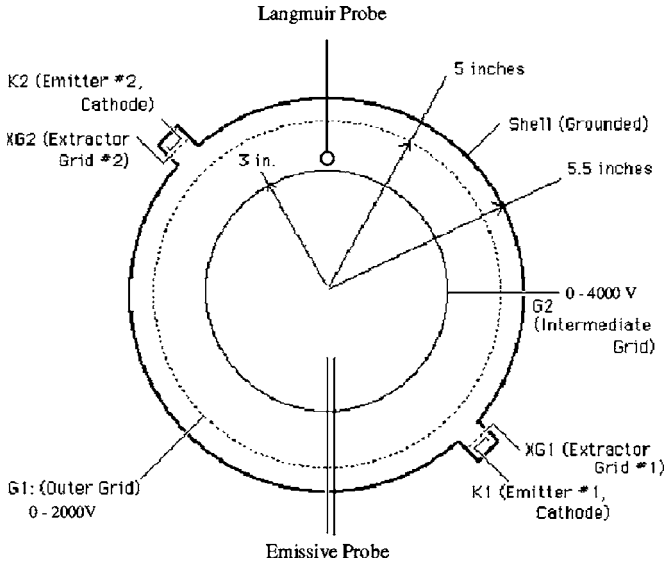


FIG. 1. Experimental setup for POPS on INS-e Device. Chamber diameter is 11 in.

well during the initial phases of compression, a bifurcation away from the static solutions is observed as the plasma becomes highly compressed. This bifurcation shortly precedes a breakdown in the formalism when part of the distribution function becomes negative (unphysical). In Sec. IV, the physical and unphysical regions of the distribution function are determined as a function of the formalism's controlling parameters, namely the electron injection energy normalized to the potential well depth, the radial scale parameter of the Gaussian density profile, and the ratio of the ion to the background electron density at the center of the sphere,  $r=0$ . Results indicate that there are limits on the achievable compressions with exact space charge neutralization that are due to geometrical convergence (in spherical geometry). However, approximate space charge neutralization is still possible in spherical and cylindrical systems; two-dimensional compressions in cylindrical systems eliminate the neutralization issue altogether. Section V discusses applications to quasineutral steady-state plasmas. For these plasmas, exact spherical solutions exist provided that the density profile is sufficiently broad. Conclusions are presented in Sec. VI.

## II. ELECTRON INJECTION FORMALISM

Both POPS and steady-state plasma schemes rely on maintaining a uniform charge density background resulting in a harmonic-oscillator potential for the ions. However, large ion compressions will disturb this harmonic potential by building up the space charge at the center of the device. To mitigate these space charge effects and preserve the harmonic-oscillator potential, additional electrons are needed. The ions have a Gaussian spatial distribution at all times. Thus, the desired electron spatial distribution is the sum of a Gaussian and a constant, the constant distribution providing the harmonic-oscillator potential. This desired spatial distribution is achieved by injecting electrons from the boundary with the proper velocity distribution. In this sec-

tion, we derive the boundary velocity distribution that will result in space charge neutralization of the ions and a harmonic-oscillator potential.

The electron density can be expressed as

$$n_e(\mathbf{r}) = \int f(\mathbf{r}, \mathbf{v}) d^3\mathbf{v}, \quad (1)$$

where  $f(\mathbf{r}, \mathbf{v})$  is the velocity distribution function (bold face denotes a vector quantity). Following the formalism of Ref. 20 (see also Appendix A), Eq. (1) can be expressed as

$$n_e(r) = \frac{4\pi}{r^2 m_e^3} \int_{-e\varphi(r)}^{\infty} dE \int_0^{L_M} dL \frac{L f(E, L)}{\sqrt{2(E + e\varphi)/m_e - L^2/r^2 m_e^2}}, \quad (2)$$

where

$$\varphi(r) = \varphi_0 \left[ 1 - \left( \frac{r}{a} \right)^2 \right], \quad \varphi_0 = - \left( \frac{en_{e0} a^2}{6\epsilon_0} \right) < 0. \quad (3)$$

In Eqs. (2) and (3),  $E$  and  $L$  are the total energy and the angular momentum of the injected electrons,  $e$  is the magnitude of the electron charge,  $\epsilon_0$  is the electrical permittivity of vacuum,  $a$  is the virtual cathode radius,  $m_e$  is the electron mass, and  $n_{e0} \equiv n_e - n_i$  is the electron density forming the uniform density virtual cathode. It has been assumed that the solutions have spherical symmetry so that  $r$  is the radius, and the velocity has a symmetry in the tangential component so that the only two significant components are the radial velocity,  $v_r$ , and the tangential velocity,  $v_{\perp}$ . The transformation from Eq. (1) to Eq. (2) is from velocity space ( $v_r, v_{\perp}$ ) to energy-angular momentum space, ( $E, L$ ). For gridded IEC plasmas, the injected electrons are monoenergetic (to lowest order) since they are accelerated through a series of grids (see Fig. 1). Consequently, the velocity distribution function can be expressed as

$$f(E, L) = \delta(E - E_0) g(E_0, L). \quad (4)$$

The electron density can now be written as

$$\begin{aligned} n_e(r) &= \frac{4\pi}{r^2 m_e^3} \int_0^{L_M(r)} dL \frac{L g(E_0, L)}{\sqrt{L_M^2/r^2 m_e^2 - L^2/r^2 m_e^2}} \\ &= \frac{4\pi}{r m_e^2} \int_0^{L_M(r)} dL \frac{L g(E_0, L)}{\sqrt{L_M^2 - L^2}}, \end{aligned} \quad (5)$$

where

$$L_M(r) \equiv m_e r \sqrt{\frac{2[E + e\varphi(r)]}{m_e}} \quad (6)$$

is the maximum angular momentum at a given radius. Equations (3) and (6) can be rearranged so that

$$\begin{aligned} r &= \frac{a}{\sqrt{2}} \sqrt{\sqrt{\left(1 + \frac{E_0}{e\varphi_0}\right)^2 - \frac{2L_M^2(r)}{m_e e\varphi_0 a^2}} + \left(1 + \frac{E_0}{e\varphi_0}\right)} \\ &= \frac{a}{\sqrt{2}} \sqrt{\sqrt{\mathcal{E}^2 + y} - \mathcal{E}}, \end{aligned} \quad (7)$$

where the following definitions have been used:  $y$

$\equiv 2L_M^2/m_e a^2 e |\varphi_0|$  and  $\mathcal{E} \equiv E_0/e |\varphi_0| - 1$ . Substituting (7) into (5) and changing the integration variable from  $L$  to  $x = 2L^2/m_e a^2 e |\varphi_0|$  yields

$$\sqrt{\mathcal{E}^2 + y} - \mathcal{E} n_e(y) = \frac{2\pi\sqrt{E_0}}{m_e^{3/2}\sqrt{\mathcal{E}+1}} \int_0^y dx \frac{g(E_0, x)}{\sqrt{y-x}}. \quad (8)$$

Equation (8) can then be solved for  $g(E_0, x)$  by an inverse Abel transform<sup>22</sup> to yield

$$g(E_0, x) = \frac{m_e^{3/2}\sqrt{\mathcal{E}+1}}{2\pi^2\sqrt{E_0}} \frac{d}{dx} \int_0^x dy \frac{n_e(y)\sqrt{\sqrt{\mathcal{E}^2+y}-\mathcal{E}}}{\sqrt{x-y}}. \quad (9)$$

The value of  $x$  is maximal when the total energy  $E_0$  is injected tangentially; in this case, it is easily found that  $x_{\max} = 4(\mathcal{E}+1)$ .

This form of the integral can then be used to determine the required injected electron distribution function on the boundary. The density can be expressed as

$$n_e(r) = n_{e0} + n_{i0} e^{-r^2/2\sigma^2}. \quad (10)$$

The second term in (10) space charge neutralizes the Gaussian ion distribution, hence the notation  $n_{i0}$ . Equation (7) is then substituted into Eq. (10) to calculate  $n_e(y)$ .

### III. SPACE CHARGE NEUTRALIZATION

In this section, the formalism of Sec. II is applied to the simulation of a POPS compression.

#### A. Small potential well limit

As a test of the ENNF code used in the next section, it is useful to explore the small potential well limit, i.e.,  $e|\varphi_0|/E_0 \rightarrow 0$ . In dimensionless variables, the limit of  $\mathcal{E} \rightarrow \infty$  in Eq. (9) is taken. Equation (9) can be written as

$$g(E_0, x) = \frac{m_e^{3/2}}{2\pi^2\sqrt{E_0}} \frac{d}{dx} \int_0^x dy \frac{n_e(y)\sqrt{\sqrt{1+y/\mathcal{E}^2}-1}}{\sqrt{1/\mathcal{E}^2}\sqrt{x-y}}, \quad (11)$$

where  $\mathcal{E} \gg 1$  has been used. Note that in this limit  $y/\mathcal{E}^2 \sim 2L_M e |\varphi_0|/m_e a^2 E_0 \rightarrow 0$  so that in this limit the integrand in (11) results in the indefinite form 0/0. Consider the case of uniform electron density profile and set  $n_e(y) = n_{e0}$ . Now expand the integrand of Eq. (11) in the small parameter  $1/\mathcal{E}^2$ . First,

$$\sqrt{1 + \frac{y}{\mathcal{E}^2}} \approx 1 + \frac{1}{2} \frac{y}{\mathcal{E}^2} - \frac{1}{8} \frac{y^2}{\mathcal{E}^4} + \dots \quad (12)$$

Substituting (12) into (11) yields

$$g(E_0, x) = \frac{m_e^{3/2} n_{e0}}{2\pi^2\sqrt{E_0}} \frac{d}{dx} \int_0^x dy \frac{\sqrt{y/2 - y^2/8\mathcal{E}^2 + \dots}}{\sqrt{y-x}}. \quad (13)$$

Keeping only the first term in the square root in the numerator of the integrand in (13) yields

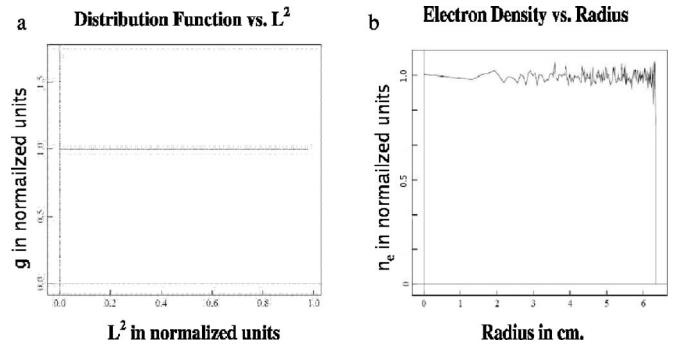


FIG. 2. Left panel: injected electron distribution function. Right panel: electron density profile.

$$g(E_0, x) = \frac{m_e^{3/2} n_{e0}}{2\sqrt{2}\pi^2\sqrt{E_0}} \frac{d}{dx} \int_0^x dy \frac{\sqrt{y}}{\sqrt{x-y}} = \frac{m_e^{3/2} n_{e0}}{4\pi\sqrt{2E_0}}, \quad (14)$$

where the integral equals  $\pi x/2$ . The remaining terms in the expansion of (13) contain numerical factors, powers of  $1/\mathcal{E}^2$ , and finite contributions from integrals of the form

$$\int_0^x dy \frac{y^{k+1/2}}{\sqrt{x-y}} = \frac{(2k+1)!!}{(2k+2)!!} \pi x^{k+1}, \quad k = 1, 2, 3, \dots \quad (15)$$

Therefore, taking the limit  $\mathcal{E} \rightarrow \infty$  renders all terms zero except the term given in Eq. (14). Thus, in the small potential well limit the distribution of injected electron on the boundary is a constant independent of the angular momentum.

This result has been tested in the ENNF code. Equation (9) has been incorporated as a boundary condition for the electrons, and the code has been run to steady-state to see if it finds the solutions. The small limit potential well is achieved by setting the force on the electrons equal to zero. Results are shown in Fig. 2. Figure 2(a) shows the applied edge distribution function. ENNF does find the steady-state solution, as evidenced by the constant electron density profile, Fig. 2(b).

#### B. Arbitrary potential well depth

In principle, Eq. (8) can be used to generate arbitrary, time-dependent electron density profiles. However, for this to be true, three conditions have to be satisfied. First of all, time dependence has to be slower than the radial electron transit times. Second, the solutions to Eq. (11) have to be physical, namely,  $g(E_0, L) \geq 0$  for all values of  $E_0, L$ . Third, even if the steady-state solutions exist, the plasma needs to find them. The preferred solutions may instead be time-dependent (dynamic).<sup>17</sup>

The ENNF code has been modified to include the behavior of the ions during plasma compressions by programming the electron injection at the boundary such that the ions will follow the self-similar solutions of Ref. 14. Although the original self-similar solutions are derived for infinite systems, previous ENNF simulations have shown that these solutions are a reasonable approximation for finite systems as well.<sup>21</sup> Therefore, considering an infinite system, Eq. (10) becomes

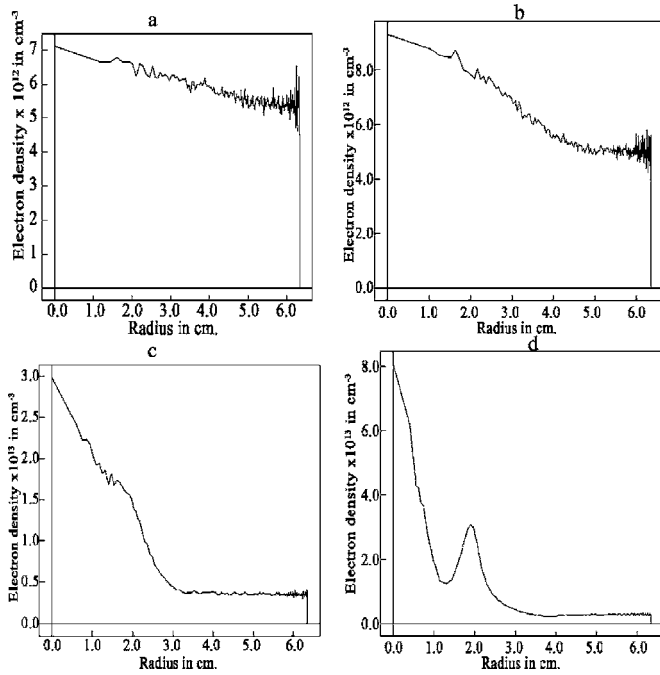


FIG. 3. Time sequence for the electron density profile.

$$n_e(r) = n_{e0} + n_{i00} e^{-r^2/2\sigma^2} \left( \frac{\sigma_0}{\sigma(t)} \right)^3 \quad (16)$$

with  $\sigma_0 \equiv \sigma(t=0)$  ( $\sigma_0 < a$ ),  $n_{i00} \equiv n_{i0}(t=0)$ . The steady-state solutions result when  $\sigma(t) = \sigma_0 = \text{const}$ . From Ref. 14, the equation of motion for  $\sigma(t)$  is

$$\frac{d^2\sigma}{dt^2} + \frac{e^2 n_{e0}}{3m_i \epsilon_0} \sigma = \frac{k_B T_{00} \sigma_0^2}{m_i \sigma^3}, \quad (17)$$

where  $m_i$  is the ion (deuterium) mass,  $k_B$  is Boltzmann's constant, and  $T_{00}$  is the ion temperature when  $\sigma = \sigma_0$ .

Figures 3(a)–3(d) show a time sequence for the electron density profiles. The corresponding sequence for the ion density is shown in Figs. 4(a)–4(d). Figures 5(a)–5(d) show the same sequence for the radial electric field profiles, while Fig. 6 shows the time sequence for the corresponding potential profiles. The solutions follow the self-similar solutions quite well until frame (c) of Figs. 3–6. This is demonstrated by the linear behavior of the electric field in Figs. 5(a) and 5(b), which shows that the potential profiles in Figs. 6(a) and 6(b) must be parabolas (harmonic-oscillator potentials). However, in frame (c) of Figs. 5 and 6, the solutions are starting to depart from the solutions derived above, and by frame (d) they have departed altogether. Figures 7(a)–7(d) show the edge distribution functions for the injected electrons and also demonstrate why the plasma departs from the self-similar solutions at the later times [frames (c) and (d)]. Note that in Fig. 7(c), a minimum has developed in the edge distribution function and this minimum is almost zero. Negative distribution functions are unphysical and the plasma departs from the self-similar solutions (and becomes dynamic) as the prescribed edge distribution function approaches zero for a finite value of  $L^2$ . In Fig. 7(d), the distribution function has become negative (the code truncates the distribution to zero

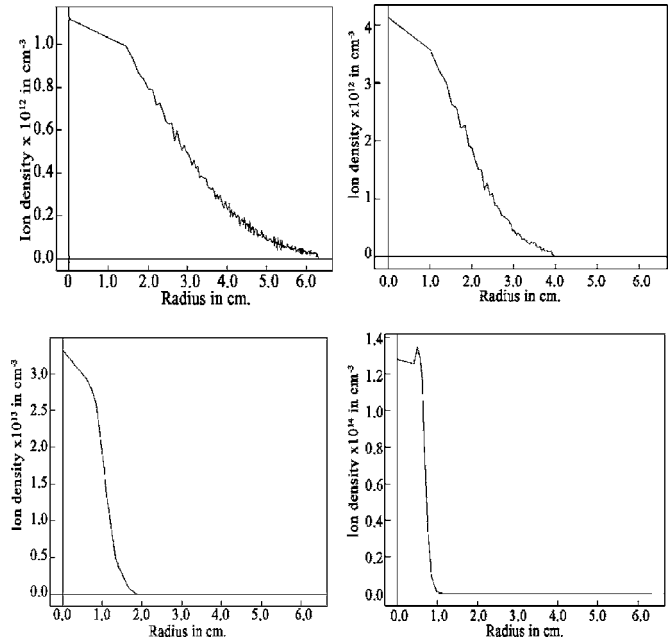


FIG. 4. Time sequence for the ion density corresponding to the electron density sequence shown in Fig. 3.

when this happens). Note that the ion compression ratio from the initial time, Fig. 4(a), and frame (c) is approximately 3.

#### IV. NEGATIVE DISTRIBUTION FUNCTION REGIONS

In Appendix B it is shown that using the electron distribution (16) in Eq. (9),  $g(E_0, x)$  can be cast in the form

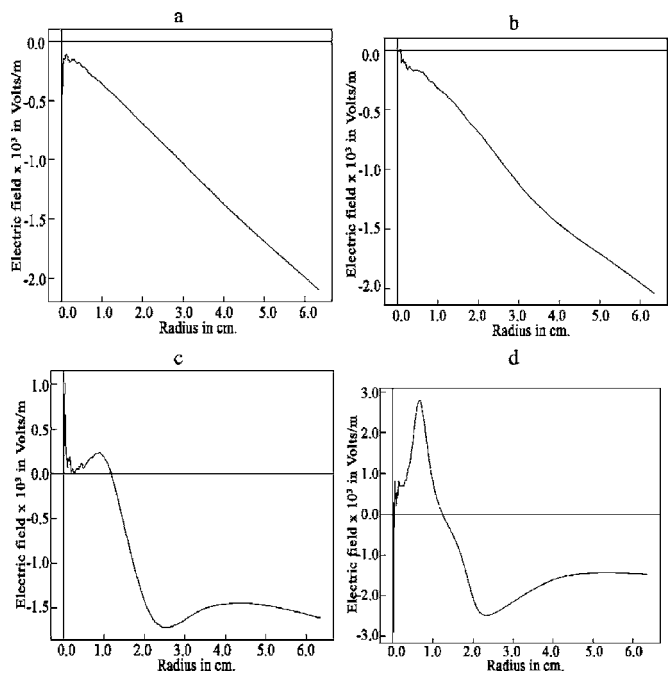


FIG. 5. Time sequence for the radial electric field corresponding to the electron density sequence shown in Fig. 3.

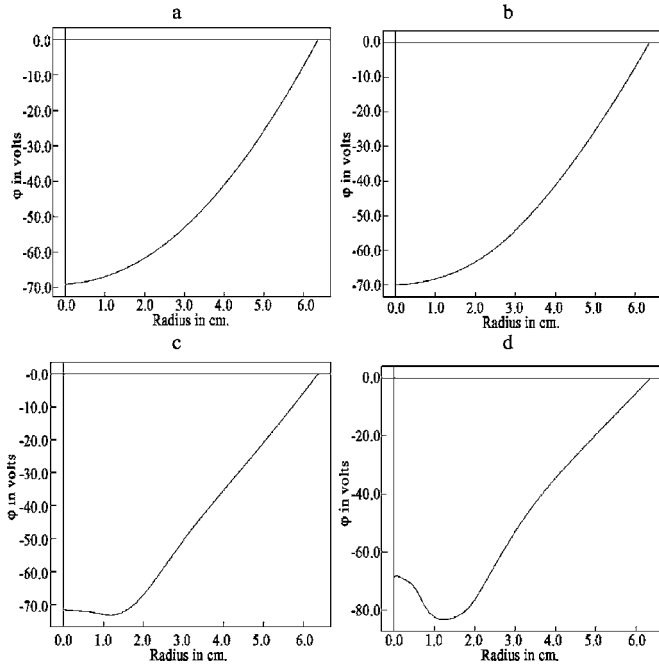


FIG. 6. Time sequence for the potential profiles corresponding to the electron density sequence shown in Fig. 3.

$$g(E_0, x) = \frac{m_e^{3/2} n_{e0} \sqrt{\mathcal{E} + 1}}{\pi^2 a \sqrt{2E_0}} \int_0^x dy \frac{1}{\sqrt{x-y}} \frac{dr(y)}{dy} \times \left\{ 1 + \eta[\sigma_0/\sigma(t)]^3 \left[ 1 - \frac{r^2(y)}{\sigma^2(t)} \right] e^{-r^2(y)/2\sigma^2(t)} \right\}, \quad (18)$$

where  $r(y)$  is given by (7) and  $\eta \equiv n_{i00}/n_{e0}$ . Note that the expression in the square brackets in (18) becomes negative for small  $\sigma(t)$  (i.e., for large compression ratios,  $\sigma_0/\sigma$ ). Al-

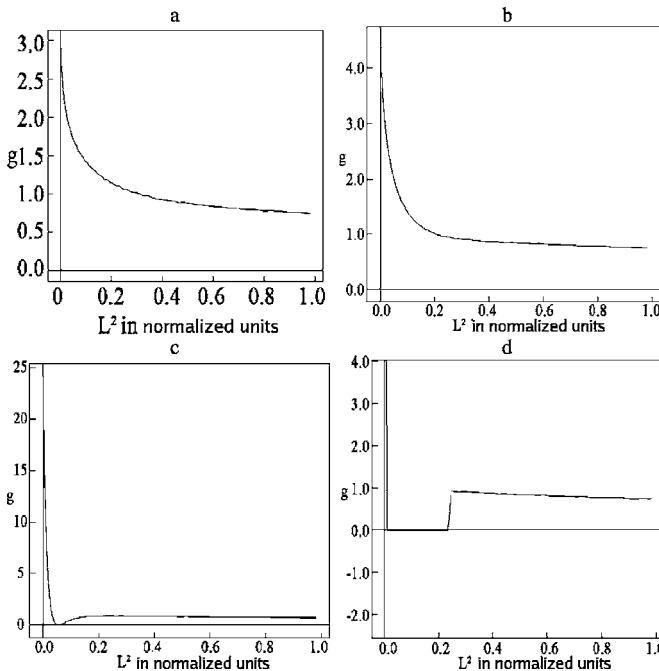


FIG. 7. Time sequence for the edge distribution function corresponding to the electron density sequence shown in Fig. 3.

though the integral expression (18) is difficult to evaluate analytically, it is desirable to understand when  $g(E_0, x)$  becomes negative as a function of the parameters  $\eta$ ,  $\mathcal{E}$ , and  $\sigma/a$  for any value of the angular momentum  $x$ . The condition  $g(E_0, x) = 0$  defines a surface in the parameter space  $(\eta, \mathcal{E}, \sigma/a)$ . Therefore, scanning over all values of  $x$  and plotting the envelope of all such surfaces describes the “forbidden” region, i.e., where  $g \leq 0$ . For qualitative understanding of the behavior of  $g(E_0, x)$ , consider the expression in the curly brackets in (18),

$$P(u) \equiv 1 + \alpha(1 - u^2)e^{-u^2/2}, \quad (19)$$

where by definition  $\alpha \equiv \eta[\sigma_0/\sigma(t)]^3$  and  $u \equiv r/\sigma$ , both positive quantities. Since the other two multiplicative factors of the integrand in (18) are positive, negative  $P(u)$  indicates a possibility of negative  $g$ . The range of values of  $u$  is  $[0, \infty)$ . The function  $P(u)$  has a minimum at  $u = \sqrt{3}$ . Since  $P(0) = 1 + \alpha$ ,  $P(\sqrt{3}) = 1 - 2\alpha e^{-3/2}$ , and  $P(\infty) = 1$ ,  $P(u)$  is always positive if  $\alpha < e^{3/2}/2$ , or

$$\eta[\sigma_0/\sigma(t)]^3 < \frac{e^{3/2}}{2} \approx 2.24. \quad (20)$$

It follows that if condition (20) is satisfied,  $g(E_0, x)$  is always positive. On the other hand, if (20) is not satisfied,  $g(E_0, x)$  may become negative. Note that (20) is independent of  $\mathcal{E}$ , and therefore valid for all  $\mathcal{E}$ . From (20),  $\sigma \sim \eta^{1/3}$ . Now consider the limit  $\mathcal{E} \gg 1$ . From Eq. (7), one obtains

$$r^2(y) = \frac{a^2}{2}(\sqrt{\mathcal{E}^2 + y} - \mathcal{E}) \approx \frac{a^2 y}{4\mathcal{E}}, \quad (21)$$

$$\frac{dr(y)}{dy} = \frac{a}{4\sqrt{2}\sqrt{\mathcal{E}^2 + y} \sqrt{\sqrt{\mathcal{E}^2 + y} - \mathcal{E}}} \approx \frac{a}{4\sqrt{\mathcal{E}y}}.$$

Substituting (21) into (18) yields

$$g(E_0, x) \approx \frac{m_e^{3/2} n_{e0}}{4\pi^2 \sqrt{2E_0}} \int_0^x dy \frac{1}{\sqrt{y(x-y)}} \left[ 1 + \eta[\sigma_0/\sigma(t)]^3 \times \left( 1 - \frac{y}{4\mathcal{E}(\sigma/a)^2} \right) e^{-y/8\mathcal{E}(\sigma/a)^2} \right] = \frac{m_e^{3/2} n_{e0}}{4\pi \sqrt{2E_0}} \left\{ 1 + \alpha \left[ \left( 1 - \frac{x}{8\mathcal{E}(\sigma/a)^2} \right) I_0 \left( \frac{x}{16\mathcal{E}(\sigma/a)^2} \right) + \frac{x}{8\mathcal{E}(\sigma/a)^2} I_1 \left( \frac{x}{16\mathcal{E}(\sigma/a)^2} \right) \right] e^{-x/16\mathcal{E}(\sigma/a)^2} \right\}, \quad (22)$$

where  $I_0$  and  $I_1$  are the modified Bessel functions<sup>23</sup> of order 0 and 1, respectively, and  $\alpha$  has the same definition as in Eq. (19). [Setting  $\alpha = 0$  in (22) yields Eq. (14).] Consider the expression in the curly brackets in (22),

$$Q(w) \equiv 1 + \alpha[(1 - 2w)I_0(w) + 2wI_1(w)]e^{-w}, \quad (23)$$

where  $w \equiv x/16\mathcal{E}(\sigma/a)^2$ . The expression in the square brackets in (23) is positive for values  $w \leq 0.8$ . Therefore, when

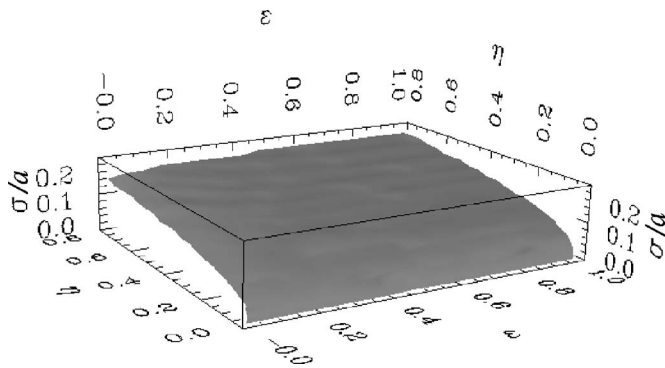


FIG. 8. Negative regions of edge distribution function for  $\sigma_0=0.5$ . Below the surface  $g(E_0, x)$  becomes negative for some  $x$ .

$$\sigma/a > \frac{1}{2\sqrt{0.8}} \approx 0.56, \quad (24)$$

(calculated at  $x=x_{\max} \approx 4\mathcal{E}$ ) the edge distribution function is always positive. On the other hand, if  $w > 0.8$ , the expression in the square brackets attains a minimum of  $-0.078$  at  $w \approx 1.45$ ; for larger  $w$  this expression remains negative and vanishes as  $w \rightarrow \infty$ . Therefore,  $g(E_0, x)$  is always positive if

$$\eta[\sigma_0/\sigma(t)]^3 < \frac{1}{0.078} \approx 12.8. \quad (25)$$

Condition (25), similarly to (20), is independent of  $\mathcal{E}$  and is therefore valid for all values of  $\mathcal{E}$  in the  $\mathcal{E} \gg 1$  limit. Not surprisingly, condition (25) is also considerably less restrictive than (20). For example, for a compression ratio of  $\sigma_0/\sigma=10$ , condition (20) requires  $\eta < 2.24 \times 10^{-3}$  whereas condition (25) requires  $\eta < 1.28 \times 10^{-2}$ , a difference of about a factor of 6. Condition (24) makes operation in the POPS regime impractical.

The surface  $g=0$ , evaluated numerically for the value of  $\sigma_0/a=0.5$ , is shown in Fig. 8. Below the surface  $g(E_0, x)$  becomes negative for some value of  $x$ . The dependence of  $\sigma/a$  on the potential well depth in the range  $\mathcal{E} \in [0, 1]$  is weak. Deeper potential wells (small  $\mathcal{E}$ ) allow for slightly higher compression ratios. Once the asymptotic regime in  $\mathcal{E}$  ( $\mathcal{E} \gg 1$ ) is reached, Eq. (25) provides a good estimate for the physical parameter range. Comparing this theory with the numerical results, from Figs. 3(a) and 4(a) one finds  $\eta \approx 0.15$  and from Fig. 6  $\mathcal{E} \approx 0.14$ . The edge distribution function becomes negative by frame (c) of Fig. 7. The compression ratio between frames (a) and (c) of Fig. 4 is about 3. Compare this with the value where  $g$  becomes negative for the same values of  $\eta$  and  $\mathcal{E}$  in Fig. 8: at this point  $\sigma/a \approx 0.1$  so the compression ratio  $\sigma_0/\sigma \approx 5$ . This is good agreement, particularly considering the fact that the behavior of the system by frame (c) has departed from the self-similar solution on which basis Fig. 8 was produced.

The above analysis shows that there are compression/density limits for space charge neutralized oscillations. Although higher compressions can be achieved with smaller ion-to-electron density ratios, the limit still exists. The case

of purely radial electron flow was originally solved by Langmuir and Blodgett.<sup>24</sup> In the limit of  $\mathcal{E} \gg 1$ , the electron density profile scales as

$$n_e(r) \sim 1/r^2. \quad (26)$$

Comparing this profile with Eq. (10), one can see that while the desired profile falls off exponentially, the profile given by Eq. (26) decreases geometrically. Consequently, if  $1/(\sigma/a)$  is large enough, the density described by Eq. (10) decreases faster than  $1/r^2$  even for the case of pure radial flow. Therefore, if the desired profile has gradients that are too steep near  $r=a$ , these profiles cannot be physically achieved; in other words, the reason for the limits is not electron repulsion, but rather it is geometrical convergence. However, earlier studies<sup>17</sup> have shown that significant improvements in plasma compression can be achieved by properly programming the distribution function *and* the energy of the electrons. What cannot be done is to simultaneously completely mitigate space charge effects with large compressions and maintain a pure harmonic-oscillator potential in a sphere.

Since the force on a particle depends only on the total enclosed charge, space charge effects can be mitigated for all of the plasma except for the tail of the Gaussian density profile. As a consequence, the plasma will depart from local thermal equilibrium during the final collapse phase. The most likely result of this is ion heating and raising of the adiabat.

It is also possible to get around the geometrical convergence limits altogether by using a cylindrical system rather than a spherical one. In this case, the electrons can be injected axially so geometrical convergence is not an issue. This sort of system would be ideal for a penning trap IEC, and will be explored in future work.

## V. APPLICATION TO QUASINEUTRAL PLASMAS

The results in the previous sections have important implications for producing fusion grade plasmas. Previous work<sup>15</sup> has indicated that the total fusion power scales as

$$P \sim \frac{\eta^2(\sigma_0/\sigma_{\min})^2}{a}. \quad (27)$$

That work also indicated that for  $\eta \sim 0.1$  and  $\sigma_0/a \sim 1$ ,  $\sigma_0/\sigma_{\min} \sim 1000$  was required for a reactor system. These parameters cannot be simultaneously achieved along with the constraints imposed by Eq. (20) or Eq. (25).

The present work suggests as another option the use of small compressions in the quasineutral limit  $\eta \rightarrow \infty$ . Either Eq. (20) or Eq. (25) provides the constraints, and Eq. (27) becomes

$$P \sim \frac{\eta^{4/3}}{a}. \quad (28)$$

This is a very favorable scaling, and it leads to a device that is different from that originally envisioned for POPS. For this device, the POPS oscillations are primarily a mechanism to resonantly heat the ions rather than for coherent compressions. Since the compression ratios are small, a high adiabat is required (i.e., high ion temperature when the plasma is

expanded). Unlike the standard POPS scenario, it may be possible to operate this device with a deuterium-tritium mixture.

A similar device (with nonparabolic potential well and negligible electron angular momentum) was originally studied by Elmore, Tuck, and Watson.<sup>1</sup> For this type of device, the principal issue is stability rather than equilibrium or space charge. The last section of Ref. 1 contains a simplified stability analysis where it is shown that the driving term ( $\equiv \Pi$ ) for the instability scales as

$$\Pi \sim \frac{m_e v_e^2(r) n_i(r)}{k T_i n_e(r)}. \quad (29)$$

A conservative estimate of the stability boundary is  $\Pi < 1$ . Taking into account that  $\eta \rightarrow \infty$  implies  $n_i(r)/n_e(r) \lesssim 1$ , Eq. (29) produces the stability condition

$$\frac{2[E_0 - e|\phi(r)|]}{k T_i} < 1, \quad (30)$$

where  $E_0 = m_e v_e^2(a)/2$  is the electron injection energy and  $\phi(r) < 0$  is the electric potential within the device. This indicates that there is likely a stability window in the quasineutral limit if the ion temperature is comparable to the electron injection energy. However, this stability analysis is approximate and it is likely that the actual boundary differs from the one given by Eq. (30).

It is also worth noting that the formalism presented here assumes monoenergetic electrons. While this is justified in present day experiments (the electron lifetime in these systems is shorter than either the ion-electron or electron-electron collision time), electrostatic instabilities might affect this assumption. However, one-dimensional<sup>19</sup> and two-dimensional<sup>25</sup> stability studies indicate that these modes are not a problem.

## VI. CONCLUSIONS

A formalism has been developed that describes the proper way to inject electrons from the boundary of a spherical IEC device in order to achieve a desired electron density profile. Two cases are presented: one for oscillating POPS plasmas and one for steady-state plasmas. In both cases, the goal is to space charge neutralize the ions in the system while simultaneously maintaining a harmonic-oscillator potential.

For the oscillatory plasmas, results indicate that there are absolute limits on the achievable compressions for perfect space charge neutralization. These limits are caused by geometrical convergence rather than space charge effects. They manifest themselves in the analytic formulation by causing negative (unphysical) distribution functions. In the simulations, this results in departures from the self-similar POPS solutions. There is very good agreement between these analytically derived limits and the numerical simulations.

In contrast, for the steady-state plasmas, space charge neutralization is possible even in the quasineutral limit. This scheme has very favorable fusion power scaling and uses small POPS oscillations to heat the plasma. A simplified sta-

bility analysis indicates that there is likely to be a stability window with deep potential wells for this system. Future work will address this issue.

## ACKNOWLEDGMENTS

This work was performed under the auspices of the National Nuclear Security Administration of the U.S. Department of Energy by Los Alamos National Laboratory, operated by Los Alamos National Security LLC under Contract No. DE-AC52-06NA25396.

## APPENDIX A: CHANGE OF VARIABLES

This appendix describes the transformation of variables from  $\mathbf{v}$  to  $E, L$  in formula (1),

$$\begin{aligned} n(\mathbf{r}) &= \int f(\mathbf{r}, \mathbf{v}) d^3\mathbf{v} \\ &= 2\pi \int_0^\infty dv_\perp v_\perp \int_{-\infty}^\infty dv_r f(\mathbf{r}, v_\perp, v_r) \\ &= 4\pi \int_0^\infty dv_\perp v_\perp \int_0^\infty dv_r f(\mathbf{r}, v_\perp, v_r), \end{aligned} \quad (A1)$$

where  $v_\perp$  is the tangential velocity at a point on the sphere, and  $v_r$  is the radial velocity at that point, and symmetry is assumed in the local tangential angle as well as in  $\pm v_r$ . Now the Jacobian of the transformation  $(v_\perp, v_r) \rightarrow (E, L)$  is found as follows. Write the relations

$$E = \frac{1}{2} m_e (v_\perp^2 + v_r^2) - e\phi, \quad (A2)$$

$$L = |\mathbf{r} \times (m_e \mathbf{v})| = m_e r v_\perp$$

with  $e > 0$  and  $\phi < 0$ . The Jacobian of the transformation (A2) is

$$\left| \frac{\partial(L, E)}{\partial(v_\perp, v_r)} \right| = \left| \det \begin{pmatrix} m_e r & 0 \\ m_e v_\perp & m_e v_r \end{pmatrix} \right| = m_e^2 r v_r. \quad (A3)$$

Therefore,

$$\left| \frac{\partial(v_\perp, v_r)}{\partial(E, L)} \right| = \frac{1}{m_e^2 r v_r}. \quad (A4)$$

Equations (A2) can be solved for  $v_\perp$  and  $v_r$ ,

$$v_r = \sqrt{\frac{2(E + e\phi)}{m_e} - \frac{L^2}{m_e^2 r^2}}, \quad v_\perp = \frac{L}{m_e r}. \quad (A5)$$

Substituting (A4) and the expressions (A5) into formula (A1) yields (1).

## APPENDIX B: TRANSFORMATION OF THE EDGE DISTRIBUTION FUNCTION

In this appendix, the calculations leading to formula (18) are presented. Using (7), the integral in Eq. (9) can be written as

$$\frac{\sqrt{2}}{a} \frac{d}{dx} \int_0^x dy \frac{\left\{1 + \eta[\sigma_0/\sigma(t)]^3 e^{-r^2(y)/2\sigma^2(t)}\right\} r(y)}{\sqrt{x-y}}, \quad (\text{B1})$$

where  $\eta = n_{i00}/n_{e0}$ . Noting that  $dy/\sqrt{x-y} = -2d\sqrt{x-y}$  and integrating (B1) by parts yields

$$\begin{aligned} & \frac{2\sqrt{2}}{a} \frac{d}{dx} \int_0^x dy \sqrt{x-y} \frac{d}{dr} \left\{ [1 + \eta[\sigma_0/\sigma(t)]^3 e^{-r^2/2\sigma^2(t)}] r \right\} \frac{dr(y)}{dy} \\ &= \frac{2\sqrt{2}}{a} \frac{d}{dx} \int_0^x dy \sqrt{x-y} \left\{ 1 + \eta[\sigma_0/\sigma(t)]^3 \left[ 1 - \frac{r^2(y)}{\sigma^2(t)} \right] \right. \\ & \quad \left. \times e^{-r^2(y)/2\sigma^2(t)} \right\} \frac{dr(y)}{dy}. \end{aligned} \quad (\text{B2})$$

Now differentiate (B2) with respect to  $x$ . There are two terms: one comes from differentiating the integral with respect to its upper limit and one from differentiating the integrand. The first term is evaluated at  $x=y$  and vanishes because of the factor  $\sqrt{x-y}$ . The second gives

$$\begin{aligned} & \frac{\sqrt{2}}{a} \int_0^x dy \frac{1}{\sqrt{x-y}} \left\{ 1 + \eta \right. \\ & \quad \left. \times [\sigma_0/\sigma(t)]^3 \left[ 1 - \frac{r^2(y)}{\sigma^2(t)} \right] e^{-r^2(y)/2\sigma^2(t)} \right\} \frac{dr(y)}{dy}. \end{aligned} \quad (\text{B3})$$

Substituting (B3) back into Eq. (9) gives Eq. (18).

<sup>1</sup>W. C. Elmore, J. L. Tuck, and K. M. Watson, *Phys. Fluids* **2**, 239 (1959).

<sup>2</sup>P. T. Farnsworth, U.S. Patent No. 3,358,402 (28 June 1966).

<sup>3</sup>R. L. Hirsch and G. A. Meeks, U.S. Patent No. 3,530,497 (22 September 1970).

<sup>4</sup>R. L. Hirsch, *J. Appl. Phys.* **38**, 4522 (1967).

<sup>5</sup>R. W. Bussard, *Fusion Technol.* **19**, 273 (1991).

<sup>6</sup>T. B. Mitchell, M. M. Schauer, and D. C. Barnes, *Phys. Rev. Lett.* **78**, 58 (1997).

<sup>7</sup>D. C. Barnes, T. B. Mitchell, and M. M. Schauer, *Phys. Plasmas* **4**, 1745 (1997).

<sup>8</sup>M. M. Schauer, T. B. Mitchell, M. H. Holzscheiter, and D. C. Barnes, *Rev. Sci. Instrum.* **68**, 3340 (1997).

<sup>9</sup>R. L. Hirsch, *Phys. Fluids* **11**, 2486 (1968).

<sup>10</sup>D. A. Swanson, B. E. Cherrington, and J. T. Verdeyen, *Phys. Fluids* **16**, 1939 (1973).

<sup>11</sup>W. M. Nevins, *Phys. Plasmas* **2**, 3804 (1995).

<sup>12</sup>T. H. Rider, *Phys. Plasmas* **2**, 1853 (1995).

<sup>13</sup>L. Chacon, G. H. Miley, D. C. Barnes, and D. A. Knoll, *Phys. Plasmas* **7**, 4547 (2000).

<sup>14</sup>D. C. Barnes and R. A. Nebel, *Phys. Plasmas* **5**, 2498 (1998).

<sup>15</sup>R. A. Nebel and D. C. Barnes, *Fusion Technol.* **38**, 28 (1998).

<sup>16</sup>J. Park, R. A. Nebel, S. Stange, and S. K. Murali, *Phys. Rev. Lett.* **95**, 015003 (2005).

<sup>17</sup>J. Park, R. A. Nebel, S. Stange, and S. K. Murali, *Phys. Plasmas* **12**, 056315 (2005).

<sup>18</sup>J. Park, R. A. Nebel, W. G. Rellergert, and M. D. Sekora, *Phys. Plasmas* **10**, 3841 (2003).

<sup>19</sup>R. A. Nebel, S. Stange, J. Park, J. M. Taccetti, S. K. Murali, and C. E. Garcia, *Phys. Plasmas* **12**, 012701 (2005).

<sup>20</sup>D. C. Barnes, L. Chacon, and J. M. Finn, *Phys. Plasmas* **9**, 4448 (2002).

<sup>21</sup>R. A. Nebel and J. M. Finn, *Phys. Plasmas* **7**, 839 (2000).

<sup>22</sup>A. I. Zayed, *Handbook of Function and Generalized Function Transformations*, 1st ed. (CRC, Boca Raton, FL, 1996), p. 343.

<sup>23</sup>I. S. Gradshteyn and I. M. Ryzhik, *Table of Integrals, Series, and Products*, corrected and enlarged ed. (Academic, New York, 1980), pp. 318–319.

<sup>24</sup>I. Langmuir and K. B. Blodgett, *Phys. Rev.* **22**, 347 (1923); **23**, 49 (1924).

<sup>25</sup>A. Marocchino, G. Lapenta, E. G. Evstatiev, R. A. Nebel, and J. Park, *Phys. Plasmas* **13**, 102106 (2006).